

Article

# N-Type Charge Carrier Transport Properties of BDOPV-Benzothiadiazole-Based Semiconducting Polymers

Siyu Wang <sup>†</sup>, Sultan Otep <sup>†</sup> , Joost Kimpel , Takehiko Mori and Tsuyoshi Michinobu <sup>\*</sup> 

Department of Materials Science and Engineering, Tokyo Institute of Technology, 2-12-1 Ookayama, Meguro-ku, Tokyo 152-8552, Japan; wang.s.at@m.titech.ac.jp (S.W.); otepov.s.aa@m.titech.ac.jp (S.O.); kimpel.j.aa@m.titech.ac.jp (J.K.); mori.t.ae@m.titech.ac.jp (T.M.)

<sup>\*</sup> Correspondence: michinobu.t.aa@m.titech.ac.jp; Tel.: +81-3-5734-3774

<sup>†</sup> These authors are equally contributed.

Received: 9 September 2020; Accepted: 25 September 2020; Published: 1 October 2020



**Abstract:** High-performance n-type organic semiconducting polymers are key components of next-generation organic electronics. Here, we designed and synthesized two electron deficient organic polymers composed of benzodifurandione-based oligo (*p*-phenylenevinylene) (BDOPV) and benzothiadiazole by Stille coupling polycondensation. BDOPV-benzothiadiazole-based copolymer (PBDOPV-BTT) possesses a D-A<sub>1</sub>-D-A<sub>2</sub> type backbone with intramolecular charge–transfer interactions, while PBDOPV-BTTz is an all-acceptor polymer. The former has a higher molecular weight ( $M_n$ ) of 109.7 kg·mol<sup>-1</sup> than the latter ( $M_n = 20.2$  kg·mol<sup>-1</sup>). The structural difference of these polymers was confirmed by the optical absorption spectra. PBDOPV-BTT showed a more bathochromically shifted absorption spectrum than PBDOPV-BTTz. The longer wavelength absorption of PBDOPV-BTT was due to the intramolecular charge transfer. Therefore, PBDOPV-BTT had a narrower band gap than PBDOPV-BTTz. However, this feature was not reflected by the lowest unoccupied molecular orbital (LUMO) levels. Both polymers displayed almost the same LUMO level of −3.8 eV. Accuracy of this observation was cross-verified by density functional theory (DFT) calculations. The electron-transporting properties were investigated by thin film transistors. PBDOPV-BTT showed an electron mobility ( $\mu_e$ ) of  $1.02 \times 10^{-2}$  cm<sup>2</sup> V<sup>-1</sup> s<sup>-1</sup> under the optimized annealing conditions. PBDOPV-BTTz exhibited poorer transistor performances with the optimized  $\mu_e$  of  $9.54 \times 10^{-6}$  cm<sup>2</sup> V<sup>-1</sup> s<sup>-1</sup>. Finally, the grazing-incidence wide angle X-ray scattering (GIWAXS) measurements of both polymer films revealed the higher crystallinity of PBDOPV-BTT with the edge-on orientation.

**Keywords:** BDOPV; electron transport; n-channel transistors; organic transistors

## 1. Introduction

Organic semiconducting polymers are promising candidates for the construction of low-cost and flexible electronic devices [1–11]. Ambipolar semiconducting polymers are among the most common organic semiconductors [12]. However, as they transfer both holes and electrons in thin film electronic devices, low-power consumption complementary devices such as photovoltaics and thermoelectrics have not been achieved. Tailoring of molecular design of organic semiconductors or optimization of device architectures alleviate this problem. The former is a synthetic approach, and synthetic chemists have devoted significant efforts to produce p-type semiconducting polymers with hole mobilities of over 1 cm<sup>2</sup> V<sup>-1</sup> s<sup>-1</sup>. The use of common organic dyes, such as diketopyrrolopyrrole (DPP) and isoindigo (IID), is effective for producing high-mobility p-type semiconducting polymers [13–21].

In contrast, the development and current status of n-type semiconducting polymers lag far behind the corresponding p-type counter polymers. In order to block hole injection and transport, organic chromophores with deep highest occupied molecular orbital (HOMO) levels must be introduced into the polymer backbone. At the same time, the lowest unoccupied molecular orbital (LUMO) levels should also be deep, facilitating electron injection and transport. Naphthalenediimide (NDI) is one of the chromophores satisfying such requirements. NDI-based polymers, as represented by N2200, are thus often employed as high-performance n-type semiconductors [22–33]. Previously, NDI-benzothiadiazole copolymer (pBTT in Figure 1) was synthesized with the D-A<sub>1</sub>-D-A<sub>2</sub> backbone sequence, where D represents an electron donor and an electron acceptor [34,35]. This polymer exhibited the electron-dominant ambipolar charge transport properties in the bottom-gate top-contact thin film transistor with a hole mobility ( $\mu_h$ ) of 0.19 cm<sup>2</sup> V<sup>-1</sup> s<sup>-1</sup> and electron mobility ( $\mu_e$ ) of 0.92 cm<sup>2</sup> V<sup>-1</sup> s<sup>-1</sup>. Embedding the sp<sup>2</sup>-nitrogen atom into the benzothiadiazole could form an electron-accepting imine structure and enhance the n-type character. The thin film transistor based on pPTT displayed unipolar electron transport properties with a  $\mu_e$  of 2.11 cm<sup>2</sup> V<sup>-1</sup> s<sup>-1</sup>. Furthermore, converting the benzothiadiazole moiety into a triply fused ring structure with the additional sp<sup>2</sup>-nitrogen atoms produced pSNT, which showed a significant increase in the  $\mu_e$  to 4.87 cm<sup>2</sup> V<sup>-1</sup> s<sup>-1</sup>. It is noteworthy that when the dielectric surface was functionalized with amine groups, electrons were accumulated, and the  $\mu_e$  was improved to 5.35 cm<sup>2</sup> V<sup>-1</sup> s<sup>-1</sup>. This is the previously mentioned optimization through device architecture to increase the unipolar charge transport properties.

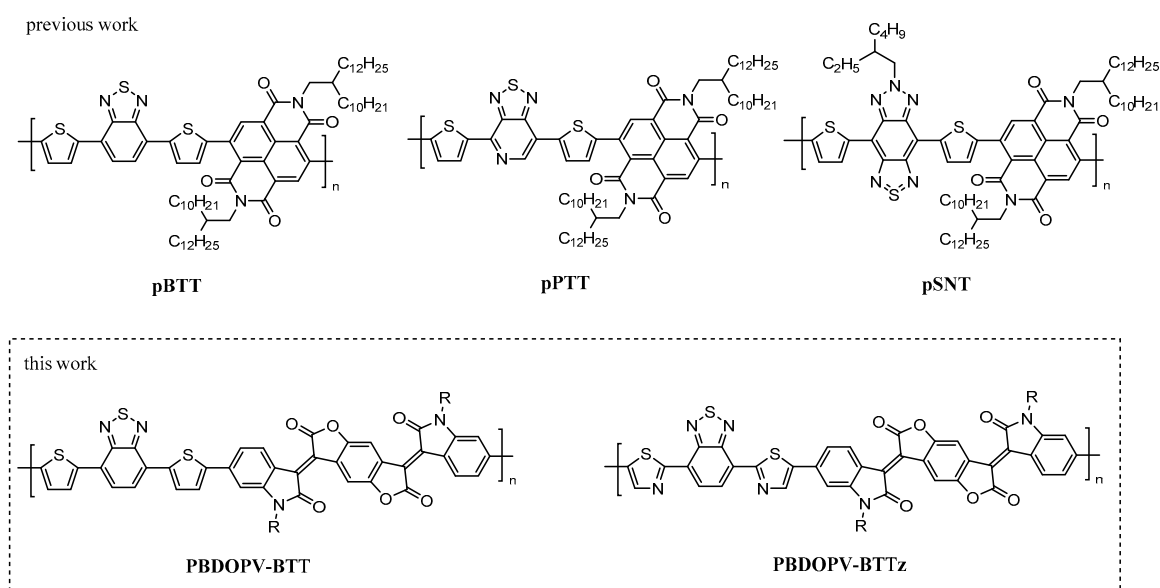


**Figure 1.** Chemical structures of high-performance naphthalenediimide (NDI)-based polymers and benzodifurandione-based oligo(*p*-phenylenevinylene) (BDOPV)-based polymers.

Although NDI is the most common building block of n-type semiconducting polymers, pursuing other electron-accepting units is scientifically significant. In this study, benzodifurandione-based oligo(*p*-phenylenevinylene) (BDOPV) is explored as another potent electron-accepting building block. There are many reports about the excellent n-channel organic transistors and n-type thermoelectronics using BDOPV-based polymers [36–46]. However, copolymers based on the BDOPV and benzothiadiazole have not yet been reported. We now report the synthesis of the BDOPV-benzothiadiazole-based copolymer (PBDOPV-BTT) with the D-A<sub>1</sub>-D-A<sub>2</sub> backbone sequence. In addition, the electron-donating thiophene was replaced by electron-accepting thiazole to produce an all-acceptor copolymer (PBDOPV-BTTz). Electron transporting properties and thin film morphology of these two polymers were investigated by thin film transistors, X-ray diffraction (XRD) analysis, and atomic force microscopy (AFM).

## 2. Materials and Methods

### 2.1. Materials and Synthesis

All chemicals were purchased from Tokyo Chemical Industry (TCI), Kanto Chemical, and Sigma Aldrich and used as received unless otherwise noted. Polymers were synthesized as follows: a mixture of BDOPV (150 mg, 0.0868 mmol), 4,7-bis(5-trimethylstannyl-2-thienyl)-2,1,3-benzothiadiazole (54.3 mg, 0.0868 mmol), Pd<sub>2</sub>(dba)<sub>3</sub> (2.4 mg, 2.6 × 10<sup>-3</sup> mmol) and P(*o*-tolyl)<sub>3</sub> (4.2 mg, 0.014 mmol) in chlorobenzene (10 mL) was refluxed at 130 °C for 36 h under nitrogen atmosphere. After cooling to room temperature, the reaction mixture was poured into methanol. After stirring for 20 min, the precipitate was collected by filtration and purified with Soxhlet extraction using methanol, acetone, hexane, a mixture of hexane and dichloromethane (10:1), and chloroform. The chloroform soluble fraction was concentrated and reprecipitated into methanol, affording PBDOPV-BTT as a dark blue solid (57.0 mg, 27.9%). Similar to this, PBDOPV-BTTz was synthesized from BDOPV (157 mg, 0.0910 mmol) and 4,7-bis(5-(trimethylstannyl)thiazol-2-yl)benzo[*c*][1,2,5] thiadiazole (80 mg, 0.091 mmol) in 51.9% yield.

### 2.2. General Measurements

Nuclear magnetic resonance (NMR) spectra were recorded using a JEOL model AL300 (300 MHz) at room temperature. Deuterated CHCl<sub>3</sub> was used as the solvent. Chemical shifts of NMR were reported in ppm (parts per million) relative to the residual solvent peak at 7.26 ppm for <sup>1</sup>H NMR spectroscopy. Coupling constants (*J*) were given in Hz. Fourier transform infrared (FT-IR) spectra were recorded on a JASCO FT/IR-4100 spectrometer in the range from 4000 to 600 cm<sup>-1</sup>. MALDI-TOF mass spectra were measured by a Shimadzu/Kratos AXIMACFR mass spectrometer equipped with a nitrogen laser (λ = 337 nm) and pulsed ion extraction, which was operated in the linear-positive ion mode at an accelerating potential of 20 kV. CHCl<sub>3</sub> solutions containing 2 g L<sup>-1</sup> of a sample, 20 g L<sup>-1</sup> of dithranol, and 1 g L<sup>-1</sup> of sodium trifluoroacetate were mixed at a ratio of 1:1:1; then, 1 μL aliquot of this mixture was deposited onto a sample target plate. Gel permeation chromatography (GPC) was measured on a JASCO GULLIVER 1500 equipped with a pump (PU-2080 Plus), an absorbance detector (RI-2031 Plus), and two Shodex GPC KF-803 columns (8.0 mm I.D. × 300 mm L) based on a conventional calibration curve using polystyrene standards. 1,2-Dichlorobenzene (40 °C) was used as a carrier solvent at the flow rate of 0.5 mL min<sup>-1</sup>. The ultraviolet (UV)-vis-near infrared (NIR) spectra were recorded on a JASCO V-670 spectrophotometer. Thermogravimetric analysis (TGA) and differential scanning calorimetry (DSC) measurements were carried out on a Rigaku TG8120 and a Rigaku DSC8230, respectively, under nitrogen flow at a scan rate of 10 °C min<sup>-1</sup>. Electrochemistry measurements were carried out on a BAS electrochemical analyzer model 612C at 20 °C in a classical three-electrode cell. The working, reference, and auxiliary electrodes were a glassy carbon electrode, Ag/AgCl/CH<sub>3</sub>CN/(*n*C<sub>4</sub>H<sub>9</sub>)<sub>4</sub>NClO<sub>4</sub>, and a Pt wire, respectively. The polymer films for electrochemical measurements were coated on the working electrode from a 1,2-dichlorobenzene solution (ca. 3 g L<sup>-1</sup>). For calibration, the redox potential of ferrocene/ferrocenium (Fc/Fc<sup>+</sup>) was measured under the same conditions, and it was located at 0.10 V vs. the Ag/AgCl electrode. Assuming that the redox potential of Fc/Fc<sup>+</sup> has an absolute energy level of -4.80 eV to vacuum, the highest occupied molecular orbital (HOMO) and lowest unoccupied molecular orbital (LUMO) energy levels were calculated according to the following equations:

$$E_{\text{HOMO}} = -(\varphi_{\text{ox}} + 4.70) \text{ (eV)} \quad (1)$$

$$E_{\text{LUMO}} = -(\varphi_{\text{red}} + 4.70) \text{ (eV)} \quad (2)$$

where  $\varphi_{\text{ox}}$  is the onset oxidation potential vs. Ag/AgCl, and  $\varphi_{\text{red}}$  is the onset reduction potential vs. Ag/AgCl.

### 2.3. Thin Film Transistors

Top-contact/bottom-gate polymer thin film transistors were fabricated on a heavily n-doped Si wafer (n<sup>+</sup>-Si) with the thermally grown SiO<sub>2</sub> layer where n<sup>+</sup>-Si and SiO<sub>2</sub> were used as the gate electrode and gate dielectric, respectively (Figure S4). The substrates were subjected to cleaning by sonication with detergent, deionized water, acetone and isopropanol for 10 min. The cleaned substrates were then treated with UV-ozone for 20 min and then modified with octadecyltrimethoxysilane (OTMS) to form a self-assembled monolayer (SAM). Thin films of the polymers were deposited on the treated substrate by spin-coating a polymer solution (ca. 3 g L<sup>-1</sup>) in 1,2-dichlorobenzene at 2000 rpm for 60 s, followed by optional thermal annealing from 150 °C to 240 °C in an Ar-filled glovebox. After polymer thin film deposition, ~40 nm thick gold was deposited as source and drain contacts using a shadow mask. The thin film transistor devices had a channel length (*L*) of 100 μm and a channel width (*W*) of 1 mm. After 1 week storage in an Ar-filled glovebox, the transistor performances were measured in a vacuum chamber (ca. 10<sup>-5</sup>–10<sup>-4</sup> mbar) using a Keithley 4200 parameter analyzer on a probe stage. The carrier mobilities, *μ*, were calculated from the data in the saturated regime according to the following equation:

$$I_{SD} = (W/2L)C_i\mu(V_{GS} - V_{th})^2 \quad (3)$$

where *I*<sub>SD</sub> is the source–drain current in the saturated regime, *W* and *L* are the semiconductor channel width and length, respectively, *C*<sub>i</sub> (*C*<sub>i</sub> = 13.7 nF cm<sup>-2</sup>) is the capacitance per unit area of the gate dielectric layer, and *V*<sub>GS</sub> and *V*<sub>th</sub> are the gate voltage and threshold voltage, respectively.

### 2.4. X-ray Diffraction

XRD patterns were obtained using a Bruker AXS D8 DISCOVER with GADDS (Cu Kα, wavelength = 0.154 nm) operated at 50 kV and 22 mA. The samples were exposed to the X-ray beam for 5 min with a sample-to-film distance of 200 mm.

### 2.5. Atomic Force Microscopy

Tapping-mode AFM measurements were performed on a Seiko Instruments SPA-400 with a Seiko Instruments DF20 cantilever.

## 3. Results and Discussion

### 3.1. Synthesis

The target polymers, PBDOPV-BTT and PBDOPV-BTTz, were synthesized by Stille coupling polycondensation (Figure 2). To ensure sufficient solubilities of the polymers, branched long alkyl chains were introduced into the BDOPV unit. Details about monomer synthesis are shown in the Supporting Information. Equimolar amounts of the benzodiadiazole and NDI monomers in chlorobenzene were refluxed at 130 °C for 36 h under nitrogen atmosphere. After purification by Soxhlet extraction with methanol, acetone, hexane, followed by a mixture of hexane and dichloromethane (10:1) to remove the impurities and low-molecular-weight fractions, PBDOPV-BTT and PBDOPV-BTTz were obtained in 27.9 and 51.9% yields, respectively. The molecular weights of chloroform extracts were evaluated by gel permeation chromatography (GPC) using polystyrene standards and 1,2-dichlorobenzene as the eluent at 40 °C. PBDOPV-BTT showed a number-average molecular weight (*M*<sub>n</sub>) of 109.7 kg·mol<sup>-1</sup> and polydispersity index (PDI) of 3.0, while PBDOPV-BTTz displayed an *M*<sub>n</sub> of 20.2 kg·mol<sup>-1</sup> and PDI of 2.4.

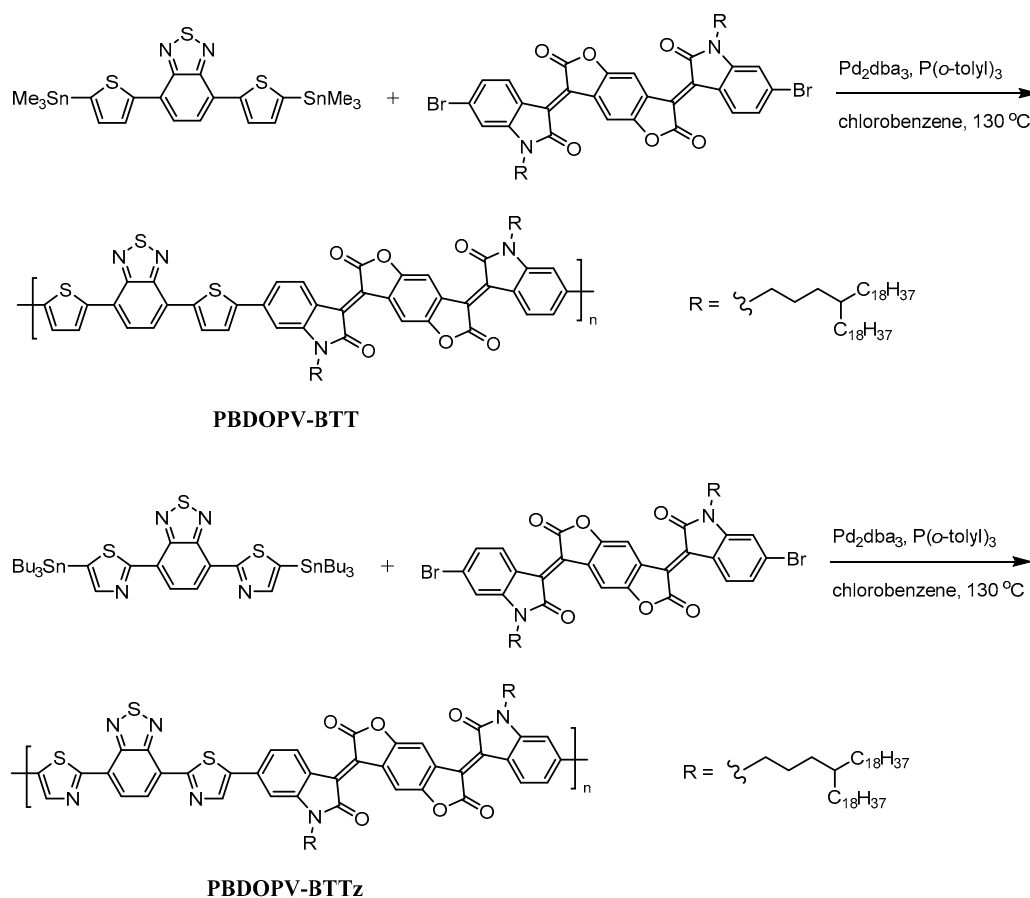


**Figure 2.** Synthesis of BDOPV-benzothiadiazole-based semiconducting polymers.

Thermogravimetric analysis (TGA) was carried out under nitrogen flow at the heating rate of  $10\text{ }^{\circ}\text{C min}^{-1}$  in order to evaluate the thermal stability of the BDOPV-benzothiadiazole-based semiconducting polymers (Figure S1). The 5% weight loss temperature ( $T_d$ ) of PBDOPV-BTT was  $396\text{ }^{\circ}\text{C}$ , while PBDOPV-BTTz showed a  $T_d$  of  $366\text{ }^{\circ}\text{C}$ . This may reflect the different molecular weights. In addition, thermal transition properties were investigated by differential scanning calorimetry (DSC). Both polymers exhibited a similar glass transition temperature ( $T_g$ ) of  $215\text{--}216\text{ }^{\circ}\text{C}$  (Figure S2). All these thermal studies suggested that they are thermally stable enough for their application.

### 3.2. Optical and Electrochemical Properties

UV-vis-NIR absorption spectra of the BDOPV-based polymers were measured. The optical absorption spectra in dilute 1,2-dichlorobenzene and as thin films are shown in Figure 3, and the data are summarized in Table 1. Both polymers showed narrow band gap absorption peaks. However, there was a noticeable difference in the peak position. PBDOPV-BTT displayed the longest wavelength absorption maximum ( $\lambda_{\text{max\_sol}}$ ) of  $836\text{ nm}$ , while the  $\lambda_{\text{max\_sol}}$  of PBDOPV-BTTz hypsochromically shifted by  $74\text{ nm}$ . This was attributed to two factors: One is an intramolecular electronic interaction. PBDOPV-BTT is composed of D-A<sub>1</sub>-D-A<sub>2</sub> repeat unit structures, and accordingly, the intramolecular charge-transfer interactions often produce a longer wavelength absorption. In contrast, PBOPV-BTTz is an all acceptor polymer that does not possess such intramolecular interactions. Secondly, an intermolecular packing interaction could have led to a shift in the absorption peak. Higher molecular weight and planar semiconducting polymers usually provide very narrow absorption bands in this film states. Since PBDOPV-BTT has much higher molecular weights than PBDOPV-BTTz, this difference may have caused the different electronic states in their thin films. The thin film spectra of the BDOPV-based polymers were indeed similar to those of the corresponding solution spectra. The as-cast films were

slightly hypsochromically shifted as compared to the solution spectra, indicating that both polymers were amorphous. The optical band gaps ( $E_g^{\text{opt}}$ ) of PBDOPV-BTT and PBDOPV-BTTz were 1.33 and 1.43 eV, respectively. However, thermal annealing resulted in the bathochromic shift of the onset wavelengths due to the partial ordering of polymer chains.

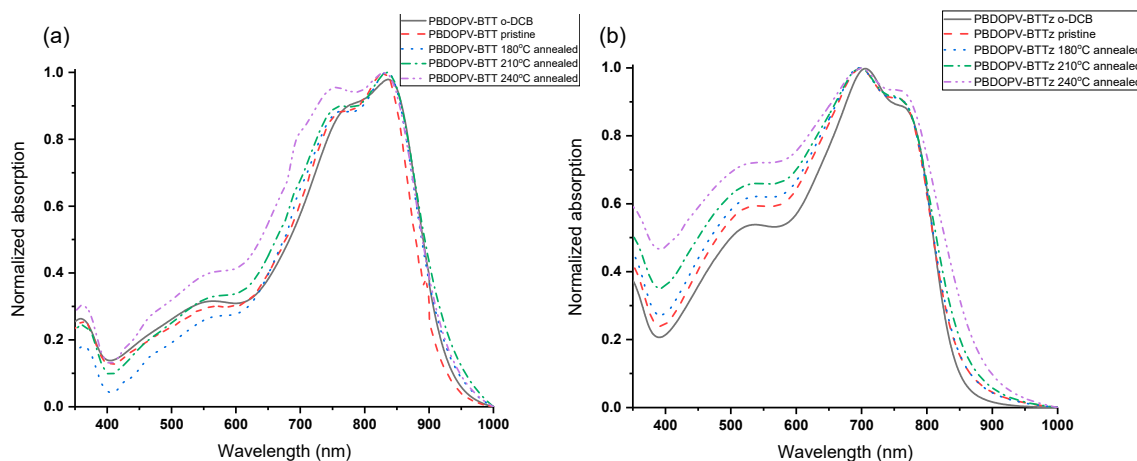


**Figure 3.** Normalized UV-vis-NIR absorption spectra of (a) PBDOPV-benzothiadiazole-based copolymer (PBDOPV-BTT) and (b) PBDOPV-BTTz in dilute 1,2-dichlorobenzene solution and thin film states with optional thermal annealing.

**Table 1.** Summary of physical properties of BDOPV-based polymers.

	$\lambda_{\text{max\_sol}}$ (nm) <sup>1</sup>	$\lambda_{\text{max\_film}}$ (nm)	$\lambda_{\text{onset}}$ (nm)	$E_g^{\text{opt}}$ (eV) <sup>3</sup>	$E_{\text{ox}}$ (V)	$E_{\text{red}}$ (V)	$E_{\text{HOMO}}$ (eV) <sup>4</sup>	$E_{\text{LUMO}}$ (eV) <sup>4</sup>	$E_g^{\text{CV}}$ (eV)
PBDOPV-BTT	836	828	930	1.33	0.85	−0.92	−5.55	−3.78	1.72
PBDOPV-BTTz	762 <sup>2</sup>	757 <sup>2</sup>	865	1.43	1.10	−0.90	−5.80	−3.80	2.00

<sup>1</sup> In 1,2-dichlorobenzene; <sup>2</sup> shoulder peak; <sup>3</sup> optical band gap ( $E_g^{\text{opt}}$ ) estimated from the onset wavelength of the as-cast films; <sup>4</sup> highest occupied molecular orbital (HOMO;  $E_{\text{HOMO}}$ ) and lowest unoccupied molecular orbital (LUMO;  $E_{\text{LUMO}}$ ) energy levels measured for the polymer thin films in  $\text{CH}_3\text{CN}$  solution with 0.1 M  $(n\text{C}_4\text{H}_9)_4\text{NClO}_4$  at the scan rate of 0.1 V s<sup>−1</sup>. For calibration, the redox potential of ferrocene/ferrocenium ( $\text{Fc}/\text{Fc}^+$ ) was measured under the same conditions, and it was 0.10 V vs. the Ag/AgCl electrode.

Cyclic voltammograms (CVs) of the polymer thin films were measured in dry  $\text{CH}_3\text{CN}$  with 0.1 M  $(n\text{C}_4\text{H}_9)_4\text{NClO}_4$ , and related data are summarized in Table 1. Both polymers displayed irreversible oxidation and reduction waves (Figure 4). Accordingly, the onset potentials were employed to estimate the frontier molecular orbital energy levels after they were calibrated with respect to the standard ferrocene/ferrocenium redox couple potential ( $\text{Fc}/\text{Fc}^+$ :  $E_{1/2} = +0.10$  V vs. Ag/AgCl). The HOMO levels ( $E_{\text{HOMO}}$ ) of both polymers, estimated from the first oxidation potentials ( $E_{\text{ox}}$ ), were slightly different. PBDOPV-BTT showed an  $E_{\text{HOMO}}$  of −5.55 eV, while the  $E_{\text{HOMO}}$  of PBDOPV-BTTz became deeper to −5.80 eV. This was reflected by the replacement of the thiophene rings of PBDOPV-BTT by the electron-accepting thiazole rings of PBDOPV-BTTz. However, the LUMO levels ( $E_{\text{LUMO}}$ ), estimated from the first reduction potentials ( $E_{\text{red}}$ ), were almost the same (−3.78 eV for PBDOPV-BTT and −3.80 eV for PBDOPV-BTTz). The current intensity of the reduction peaks of PBDOPV-BTTz was stronger than that of PBDOPV-BTT due to the all-acceptor structure.

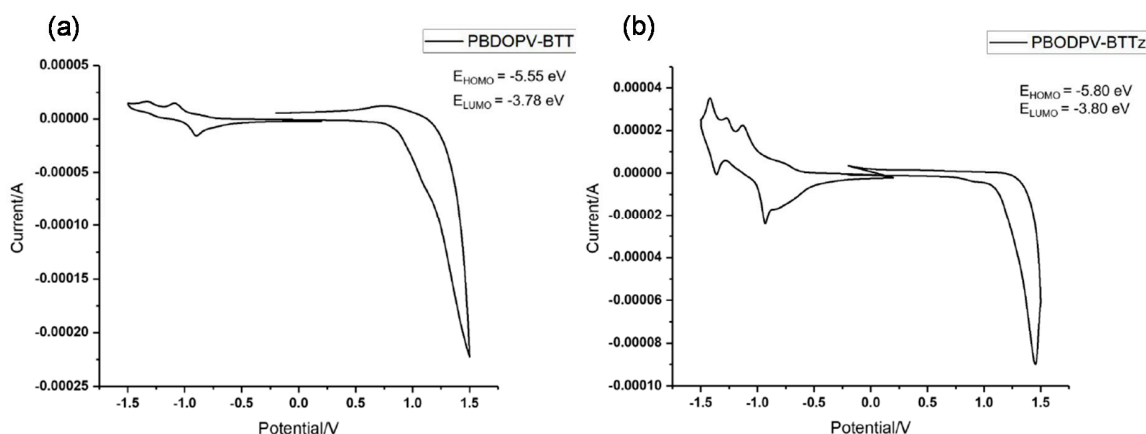


**Figure 4.** Cyclic voltammograms of (a) PBDOPV-BTT and (b) PBDOPV-BTTz films drop-cast on a glassy carbon electrode, measured in  $\text{CH}_3\text{CN}$  with 0.1 M  $(n\text{C}_4\text{H}_9)_4\text{NClO}_4$  at the scan rate of  $0.1 \text{ V s}^{-1}$ .

### 3.3. Computational Calculations

The dihedral angle between monomers and frontier orbital energy levels were computationally obtained after geometry optimization by implementing density functional theory (DFT) with the B3LYP functional and the 6-31G(d) basis set using Gaussian 16 [47]. Optimized structures of dimers, tetramers and hexamers were verified by vibrational analysis, seeing that equilibrium structures do not possess imaginary frequencies.

Dihedral angles between monomer units were analyzed as conjugation length greatly influences charge mobility and conjugation is broken at high dihedral angles. Although frontier orbital energy levels have been experimentally obtained, theoretical results will serve to reinforce these results. By incorporation of the  $\text{sp}^2$ -nitrogen atom in thiazole in PBDOPV-BTTz, it was postulated that the HOMO and LUMO energy levels would be deeper compared to PBDOPV-BTT. This hypothesis is confirmed by the UV-vis-NIR and CV results, though the difference is not substantial: a lowering of the HOMO energy level by 0.25 eV is observed, while the LUMO is only stabilized by an additional 0.02 eV. Computational calculations were used to ensure experimental observations are in line with theory. The BDOPV moiety is generally reported as flat due to its conjugation, however, it is noteworthy that both its flat and its twisted structure are stable conformers. These adopted conformers are considered in the dimers, which are denoted as A and B, respectively (Figure 5). During synthesis of the polymer and upon casting the film, either conformation is adopted, and interchange between the conformations is unlikely attributed to the high rotational energy barrier of  $150\text{--}200 \text{ kJ mol}^{-1}$  for both polymers.

Dihedral angles between monomers only had a marginal disparity for all polymers: values ranged from  $18^\circ$  to  $21^\circ$ , indicating that it is likely that conjugation is maintained between monomer units (Table S1). Calculated HOMO and LUMO energy levels were slightly higher in energy than the experimentally obtained values, however, HOMO–LUMO gaps were in good agreement with the experimental results. Although it also has coefficients on BDOPV, the HOMO energy level had the greatest coefficients and hence localized on BTT and BTTz. In contrast, the LUMO was localized exclusively on BDOPV. The HOMO energy level of PBDPOV-BTTz was roughly 0.26 eV deeper than that of PBDOPV-BTT, in line with the experiment. The LUMO energy level of PBDPOV-BTTz was roughly 0.05 eV deeper than that of PBDOPV-BTT in both stable BDOPV conformations—only a small increase in stabilization compared to experimentally obtained results (Table S2).

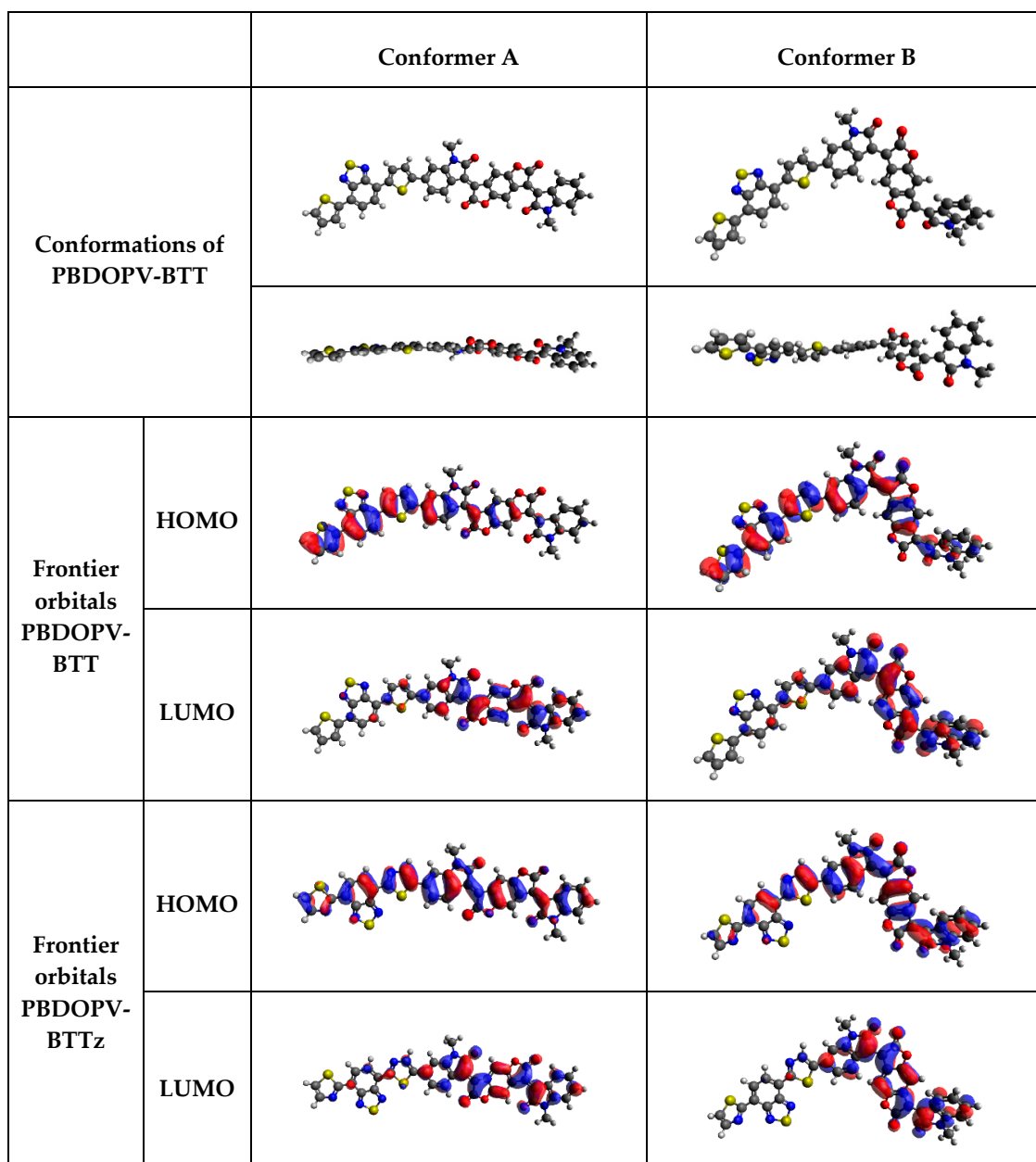


**Figure 5.** Exemplar top and side views of calculated conformations of the PBDOPV-BTT dimer (analogous for PBDOPV-BTTz). Calculated HOMO and LUMO energy surfaces of the dimer of PBDOPV-BTT and PBDOPV-BTTz (B3LYP/6-31G(d), long and branched alkyl chains are substituted by the methyl group).

#### 3.4. Thin Film Transistor Performances

Charge transport properties of BDOPV-based polymers were studied by conventional bottom-gate/top-contact thin film transistors. Although both polymers displayed electron-dominant ambipolar charge transport behavior, especially when thermal annealing temperature was not sufficiently high, we mainly focused on electron transporting behavior in this study. The transfer curves are shown in Figure 6, Figure S3-1 and Figure S3-2, and the relevant data are listed in Table 2. The electron mobilities ( $\mu_e$ ) were extracted from the saturation regime. Transistor performances were improved when the polymer films were thermally annealed. The average  $\mu_e$  of the as-cast film of PBDOPV-BTT was  $2.92 \times 10^{-3} \text{ cm}^2 \text{ V}^{-1} \text{ s}^{-1}$ . The optimized annealing temperature of this polymer was 240 °C, giving  $\mu_e$  of  $1.02 \times 10^{-2} \text{ cm}^2 \text{ V}^{-1} \text{ s}^{-1}$ . The optimized device also had an

excellent  $I_{on}/I_{off}$  ratio of  $10^3$ – $10^5$  and the smallest threshold voltage ( $V_{th}$ ) of 18 V. Despite the slightly deeper LUMO level, PBDOPV-BTTz displayed poorer electron-transporting properties compared to PBDOPV-BTT. The as-cast film of PBDOPV-BTTz exhibited a  $\mu_e$  of  $2.88 \times 10^{-6} \text{ cm}^2 \text{ V}^{-1} \text{ s}^{-1}$ . The  $\mu_e$  value gradually increased by thermal annealing, and the highest  $\mu_e$  was  $9.54 \times 10^{-6} \text{ cm}^2 \text{ V}^{-1} \text{ s}^{-1}$  at the optimized annealing temperature of 210 °C. It should be noted that the transistor measurements were carried out one week after the devices were fabricated. Although they were stored in an Ar-filled glovebox, the intrinsic instability of n-type organic semiconductors could have influenced the n-channel transistor performance.

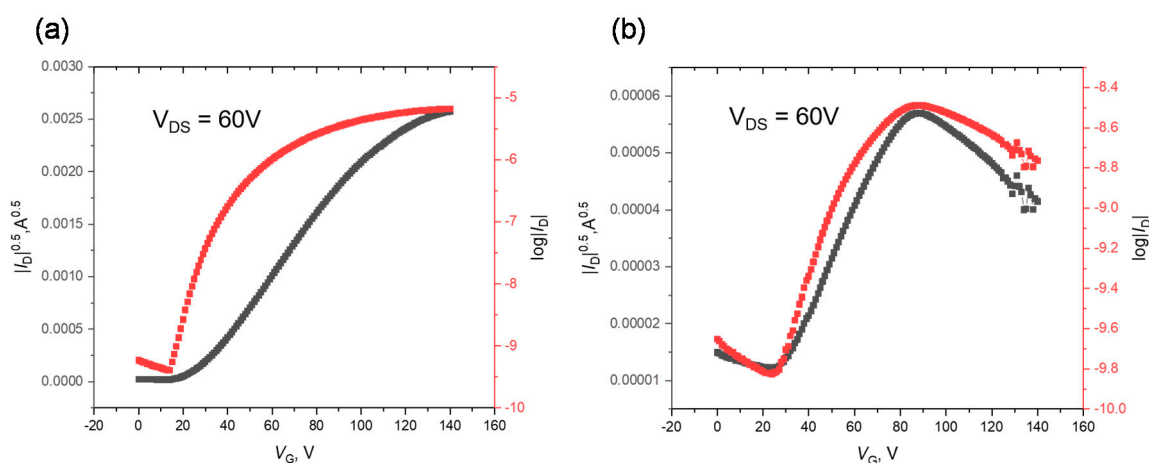


**Figure 6.** Transfer characteristics of thin film transistors based on polymer thin films of (a) PBDOPV-BTT after annealing at 240 °C and (b) PBDOPV-BTTz after annealing at 210 °C ( $L = 100 \mu\text{m}$  and  $W = 1000 \mu\text{m}$ ).

**Table 2.** Summary of thin film transistor performances (best performance hence highlighted).

	Annealing Temp. (°C)	$\mu_e \text{ max}$ ( $\text{cm}^2 \text{ V}^{-1} \text{ s}^{-1}$ )	$\mu_e \text{ average}$ ( $\text{cm}^2 \text{ V}^{-1} \text{ s}^{-1}$ ) <sup>1</sup>	$I_{on}/I_{off}$	$V_{th}$ (V)
PBDOPV-BTT	-	$5.00 \times 10^{-3}$	$(2.92 \pm 1.19) \times 10^{-3}$	$10^2$ – $10^3$	$45 \pm 7$
	150	$5.21 \times 10^{-3}$	$(3.61 \pm 1.27) \times 10^{-3}$	$10^3$ – $10^5$	$41 \pm 6$
	180	$6.44 \times 10^{-3}$	$(5.02 \pm 1.37) \times 10^{-3}$	$10^2$ – $10^4$	$27 \pm 7$
	210	$3.97 \times 10^{-3}$	$(2.24 \pm 0.78) \times 10^{-3}$	$10^3$ – $10^4$	$36 \pm 9$
	<b>240</b>	<b><math>1.25 \times 10^{-2}</math></b>	<b><math>(1.02 \pm 0.14) \times 10^{-2}</math></b>	<b><math>10^3</math>–<math>10^5</math></b>	<b><math>18 \pm 12</math></b>
PBDOPV-BTTz	-	$4.09 \times 10^{-6}$	$(2.88 \pm 0.79) \times 10^{-6}$	$10$ – $10^2$	$12 \pm 8$
	150	$4.33 \times 10^{-6}$	$(3.13 \pm 0.98) \times 10^{-6}$	10	$4 \pm 7$
	180	$7.40 \times 10^{-6}$	$(4.86 \pm 1.30) \times 10^{-6}$	$10$ – $10^2$	$13 \pm 7$
	<b>210</b>	<b><math>1.06 \times 10^{-5}</math></b>	<b><math>(9.54 \pm 0.73) \times 10^{-6}</math></b>	<b><math>10</math>–<math>10^2</math></b>	<b><math>13 \pm 10</math></b>
	240	$6.81 \times 10^{-6}$	$(4.42 \pm 1.70) \times 10^{-6}$	10	$25 \pm 13$

<sup>1</sup> Average mobilities were calculated from five devices. Errors are given as mean absolute deviation from the average values.

### 3.5. Thin Film Morphology

In order to correlate the transistor performances with polymer thin film morphology, grazing-incidence wide angle X-ray scattering (GIWAXS) measurements were performed. The polymer films were prepared by spin-coating on OTMS-treated Si/SiO<sub>2</sub> substrates and subjected to thermal annealing at optimized temperatures. PBDOPV-BTT showed some peaks in the out-of-plane direction, while there were no well-defined in-plane patterns (Figure 7a). In contrast, PBDOPV-BTTz displayed no noticeable peaks in both out-of-plane and in-plane directions, suggesting amorphous microstructures. The lamellar packing distance of PBDOPV-BTT was calculated to be 26.7 Å ( $2\theta = 3.31^\circ$ ). The other weak peaks ascribed to either higher-order, or different packing patterns provided the distance of 20.9 Å ( $2\theta = 4.23^\circ$ ) and 15.2 Å ( $2\theta = 5.83^\circ$ ). However, no  $\pi$ – $\pi$  stacking peaks were observed. All these results suggested that PBDOPV-BTT has a higher crystallinity with an edge-on orientation suitable for

transistor applications, while PBDOPV-BTTz forms an amorphous film. This difference may have been caused by the molecular weights and intermolecular interactions.

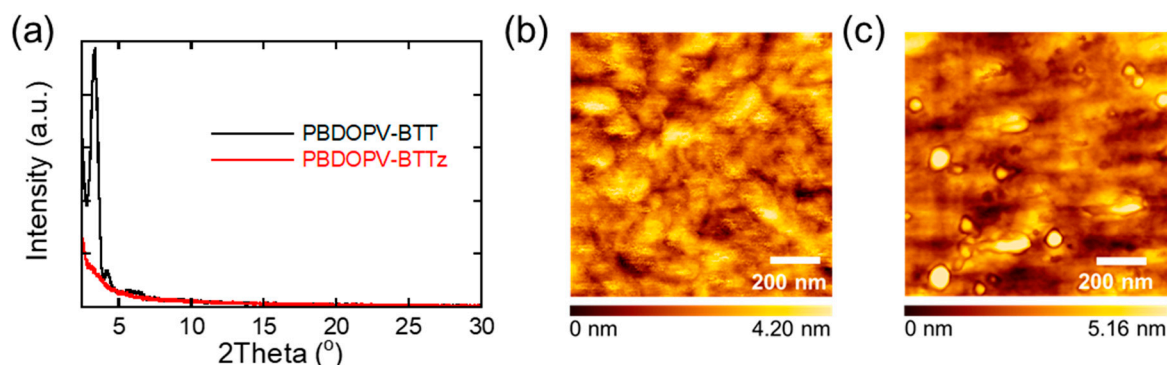


**Figure 7.** (a) Out-of-plane grazing-incidence wide angle X-ray scattering (GIWAXS) patterns of the polymer thin films of PBDOPV-BTT and PBDOPV-BTTz after thermal annealing at 240 and 210 °C, respectively. Tapping-mode atomic force microscopy (AFM) images of (b) PBDOPV-BTT and (c) PBDOPV-BTTz after thermal annealing at 240 and 210 °C, respectively.

AFM images of PBDOPV-BTT thin film prepared at optimized conditions revealed well-defined and relatively ordered separation of interconnected domains (Figure 7b), which were in good agreement with the charge transport property. Although the annealed PBDOPV-BTTz film had similar surface morphology (Figure 7c), there were isolated aggregates of up to 210 nm in width, extending from the surface to up to ~5 nm. These structures could be the result of preaggregation of the polymer in 1,2-dichlorobenzene or poor polymer-substrate interaction. Nevertheless, the presence of these large aggregates could have contributed to the limited transistor performances of PBDOPV-BTTz devices.

#### 4. Conclusions

In summary, the copolymers composed of BDOPV and benzothiadiazole units were for the first time synthesized, and their electron transporting properties were investigated by thin film transistors. The D-A<sub>1</sub>-D-A<sub>2</sub> type polymer of PBDOPV-BTT showed a higher electron mobility than the all-acceptor type PBDOPV-BTTz. This was due to the higher molecular weight and dipole-induced intermolecular interactions. All-acceptor polymers are promising molecular architectures with deep LUMO levels, but controlling the backbone planarity and intermolecular interactions is also required.

**Supplementary Materials:** The following are available online at <http://www.mdpi.com/2079-9292/9/10/1604/s1>, Figure S1: Thermogravimetric analysis (TGA) curves of the copolymers under nitrogen atmosphere at the heating rate of 10 °C min<sup>-1</sup>; Figure S2: Thermogravimetric analysis (TGA) curves of the copolymers under nitrogen atmosphere at the heating rate of 10 °C min<sup>-1</sup>; Figure S3-1: Transfer curves of thin film transistors based on PBDOPV-BTT: (a) as cast, after thermal annealing at (b) 150 °C, (c) 180 °C, (d) 210 °C, and (e) 240 °C ( $L = 100 \mu\text{m}$  and  $W = 1000 \mu\text{m}$ ); Figure S3-2: Transfer curves of thin film transistors based on PBDOPV-BTTz: (a) as cast, after thermal annealing at (b) 150 °C, (c) 180 °C, (d) 210 °C, and (e) 240 °C ( $L = 100 \mu\text{m}$  and  $W = 1000 \mu\text{m}$ ); Figure S4: Illustration of the thin film transistor structure.

**Author Contributions:** Synthesis and characterization, S.W.; transistor measurements, S.W. and S.O.; computational study, J.K.; writing—original draft preparation, T.M. (Tsuyoshi Michinobu); writing—review and editing, T.M. (Tsuyoshi Michinobu), S.O. and J.K.; supervision, T.M. (Tsuyoshi Michinobu) and T.M. (Takehiko Mori). All authors have read and agreed to the published version of the manuscript.

**Funding:** This work was supported by JSPS KAKENHI Grants 18KK0157 and 19H02786, the Asahi Glass Foundation, the Murata Science Foundation, the Iketani Science and Technology Foundation, the Precise Measurement Technology Promotion Foundation, and the Yashima Environment Technology Foundation.

**Acknowledgments:** The authors thank Open Facility Center, Tokyo Institute of Technology for assistance in GIWAXS measurements.

**Conflicts of Interest:** The authors declare no conflict of interest.

## References

1. Yao, Y.; Dong, H.; Hu, W. Charge Transport in Organic and Polymeric Semiconductors for Flexible and Stretchable Devices. *Adv. Mater.* **2016**, *28*, 4513–4523. [[CrossRef](#)] [[PubMed](#)]
2. Jiang, Y.; Guo, Y.; Liu, Y. Engineering of Amorphous Polymeric Insulators for Organic Field-Effect Transistors. *Adv. Electron. Mater.* **2017**, *3*, 1700157. [[CrossRef](#)]
3. Shi, L.; Guo, Y.; Hu, W.; Liu, Y. Design and effective synthesis methods for high-performance polymer semiconductors in organic field-effect transistors. *Mater. Chem. Front.* **2017**, *1*, 2423–2456. [[CrossRef](#)]
4. Wang, B.; Huang, W.; Chi, L.; Al-Hashimi, M.; Marks, T.J.; Facchetti, A. High-*k* Gate Dielectrics for Emerging Flexible and Stretchable Electronics. *Chem. Rev.* **2018**, *118*, 5690–5754. [[CrossRef](#)] [[PubMed](#)]
5. Nketia-Yawson, B.; Noh, Y.-Y. Recent Progress on High-Capacitance Polymer Gate Dielectrics for Flexible Low-Voltage Transistors. *Adv. Funct. Mater.* **2018**, *28*, 1802201. [[CrossRef](#)]
6. Wang, Y.; Michinobu, T. Rational design strategies for electron-deficient semiconducting polymers in ambipolar/n-channel organic transistors and all-polymer solar cells. *J. Mater. Chem. C* **2018**, *6*, 10390–10410. [[CrossRef](#)]
7. Matsuhisa, N.; Chen, X.; Bao, Z.; Someya, T. Materials and structural designs of stretchable conductors. *Chem. Soc. Rev.* **2019**, *48*, 2946–2966. [[CrossRef](#)]
8. Sun, H.; Guo, X.; Facchetti, A. High-Performance n-Type Polymer Semiconductors: Applications, Recent Development, and Challenges. *Chem* **2020**, *6*, 1310–1326. [[CrossRef](#)]
9. Guo, X.; Facchetti, A. The journey of conducting polymers from discovery to application. *Nat. Mater.* **2020**, *19*, 922–928. [[CrossRef](#)]
10. Yuvaraja, S.; Nawaz, A.; Liu, Q.; Dubal, D.; Surya, S.G.; Salama, K.N.; Sonar, P. Organic field-effect transistor-based flexible sensors. *Chem. Soc. Rev.* **2020**, *49*, 3423–3460. [[CrossRef](#)]
11. Kimpel, J.; Michinobu, T. Conjugated polymers for functional applications: Lifetime and performance of polymeric organic semiconductors in organic field-effect transistors. *Polym. Int.* **2020**. [[CrossRef](#)]
12. Zhu, X.; Zhang, S.-R.; Zhou, Y.; Han, S.-T. Ambipolar polymers for transistor applications. *Polym. Int.* **2020**. [[CrossRef](#)]
13. Li, Y.; Sonar, P.; Murphy, L.; Hong, W. High mobility diketopyrrolopyrrole (DPP)-based organic semiconductor materials for organic thin film transistors and photovoltaics. *Energy Environ. Sci.* **2013**, *6*, 1684–1710. [[CrossRef](#)]
14. Wang, E.; Mammo, W.; Andersson, M.R. 25th Anniversary Article: Isoindigo-Based Polymers and Small Molecules for Bulk Heterojunction Solar Cells and Field Effect Transistors. *Adv. Mater.* **2014**, *26*, 1801–1826. [[CrossRef](#)] [[PubMed](#)]
15. Lei, T.; Wang, J.-Y.; Pei, J. Design, Synthesis, and Structure-Property Relationships of Isoindigo-Based Conjugated Polymers. *Acc. Chem. Res.* **2014**, *47*, 1117–1126. [[CrossRef](#)] [[PubMed](#)]
16. Stalder, R.; Mei, J.; Graham, K.R.; Estrada, L.A.; Reynolds, J.R. Isoindigo, a Versatile Electron-Deficient Unit for High-Performance Organic Electronics. *Chem. Mater.* **2014**, *26*, 664–678. [[CrossRef](#)]
17. Yi, Z.; Wang, S.; Liu, Y. Design of High-Mobility Diketopyrrolopyrrole-Based-Conjugated Copolymers for Organic Thin-Film Transistors. *Adv. Mater.* **2015**, *27*, 3589–3606. [[CrossRef](#)] [[PubMed](#)]
18. Li, W.; Hendriks, K.H.; Wienk, M.M.; Janssen, R.A.J. Diketopyrrolopyrrole Polymers for Organic Solar Cells. *Acc. Chem. Res.* **2016**, *49*, 78–85. [[CrossRef](#)]
19. Liu, Q.; Bottle, S.E.; Sonar, P. Developments of Diketopyrrolopyrrole-Dye-Based Organic Semiconductors for a Wide Range of Applications in Electronics. *Adv. Mater.* **2020**, *32*, 1903882. [[CrossRef](#)]
20. Liu, Q.; Wang, Y.; Kohara, A.; Matsumoto, H.; Manzhos, S.; Feron, K.; Bottle, S.E.; Michinobu, T.; Sonar, P. Tuning the Charge Carrier Polarity of Organic Transistors by Varying the Electron Affinity of the Flanked Units in Diketopyrrolopyrrole-Based Copolymers. *Adv. Funct. Mater.* **2020**, *30*, 1907452. [[CrossRef](#)]
21. Liu, Q.; Wang, Y.; Ren, Y.; Kohara, A.; Matsumoto, H.; Chen, Y.; Manzhos, S.; Feron, K.; Bottle, S.E.; Bell, J.; et al. Diketopyrrolopyrrole-Based Dual-Acceptor Copolymers to Realize Tunable Charge Carrier Polarity of Organic Field-Effect Transistors and High-Performance Nonvolatile Ambipolar Flash Memories. *ACS Appl. Electron. Mater.* **2020**, *2*, 1609–1618. [[CrossRef](#)]
22. Yan, H.; Chen, Z.; Zheng, Y.; Newman, C.; Quinn, J.R.; Dötz, F.; Kastler, M.; Facchetti, A. A high-mobility electron-transporting polymer for printed transistors. *Nature* **2009**, *57*, 679–686. [[CrossRef](#)] [[PubMed](#)]

23. Gao, X.; Hu, Y. Development of n-type organic semiconductors for thin film transistors: A viewpoint of molecular design. *J. Mater. Chem. C* **2014**, *2*, 3099–3117. [[CrossRef](#)]
24. Wang, Y.; Michinobu, T. Benzothiadiazole and its  $\pi$ -extended, heteroannulated derivatives: Useful acceptor building blocks for high-performance donor-acceptor polymers in organic electronics. *J. Mater. Chem. C* **2016**, *4*, 6200–6214. [[CrossRef](#)]
25. Wang, Y.; Hasegawa, T.; Matsumoto, H.; Mori, T.; Michinobu, T. D-A<sub>1</sub>-D-A<sub>2</sub> Backbone Strategy for Benzobisthiadiazole Based n-Channel Organic Transistors: Clarifying the Selenium-Substitution Effect on the Molecular Packing and Charge Transport Properties in Electron-Deficient Polymers. *Adv. Funct. Mater.* **2017**, *27*, 1701486. [[CrossRef](#)]
26. Jia, H.; Lei, T. Emerging research directions for n-type conjugated polymers. *J. Mater. Chem. C* **2019**, *7*, 12809–12821. [[CrossRef](#)]
27. Wang, Y.; Hasegawa, T.; Matsumoto, H.; Michinobu, T. Significant Improvement of Unipolar n-Type Transistor Performances by Manipulating the Coplanar Backbone Conformation of Electron-Deficient Polymers via Hydrogen Bonding. *J. Am. Chem. Soc.* **2019**, *141*, 3566–3575. [[CrossRef](#)]
28. Wang, Y.; Hasegawa, T.; Matsumoto, H.; Michinobu, T. Significant Difference in Semiconducting Properties of Isomeric All-Acceptor Polymers Synthesized via Direct Arylation Polycondensation. *Angew. Chem. Int. Ed.* **2019**, *58*, 11893–11902. [[CrossRef](#)]
29. Sui, Y.; Deng, Y.; Du, T.; Shi, Y.; Geng, Y. Design strategies of n-type conjugated polymers for organic thin-film transistors. *Mater. Chem. Front.* **2019**, *3*, 1932–1951. [[CrossRef](#)]
30. Said, A.A.; Xie, J.; Wang, Y.; Wang, Z.; Zhou, Y.; Zhao, K.; Gao, W.-B.; Michinobu, T.; Zhang, Q. Efficient Inverted Perovskite Solar Cells by Employing N-Type (D-A<sub>1</sub>-D-A<sub>2</sub>) Polymers as Electron Transporting Layer. *Small* **2019**, *15*, 1803339. [[CrossRef](#)]
31. Wang, Y.; Kim, S.W.; Lee, J.; Matsumoto, H.; Kim, B.J.; Michinobu, T. Dual Imide-Functionalized Unit-Based Regioregular D-A<sub>1</sub>-D-A<sub>2</sub> Polymers for Efficient Unipolar n-Channel Organic Transistors and All-Polymer Solar Cells. *ACS Appl. Mater. Interfaces* **2019**, *11*, 22583–22594. [[CrossRef](#)] [[PubMed](#)]
32. Kim, S.W.; Wang, Y.; You, H.; Lee, W.; Michinobu, T.; Kim, B.J. Impact of Incorporating Nitrogen Atoms in Naphthalenediimide-Based Polymer Acceptors on the Charge Generation, Device Performance, and Stability of All-Polymer Solar Cells. *ACS Appl. Mater. Interfaces* **2019**, *11*, 35896–35903. [[CrossRef](#)] [[PubMed](#)]
33. Dong, J.; Wang, Y.; Mori, T.; Michinobu, T. Improving the air-stability of n-type organic thin-film transistors by polyacrylonitrile additive. *Jpn. J. Appl. Phys.* **2020**, *59*, SDDC05. [[CrossRef](#)]
34. Zhao, Z.; Yin, Z.; Chen, H.; Zheng, L.; Zhu, C.; Zhang, L.; Tan, S.; Wang, H.; Guo, Y.; Tang, Q.; et al. High- Performance, Air-Stable Field-Effect Transistors Based on Heteroatom-Substituted Naphthalenediimide-Benzothiadiazole Copolymers Exhibiting Ultrahigh Electron Mobility up to 8.5 cm<sup>2</sup> V<sup>-1</sup> s<sup>-1</sup>. *Adv. Mater* **2017**, *29*, 1602410. [[CrossRef](#)] [[PubMed](#)]
35. Wang, Y.; Hasegawa, T.; Matsumoto, H.; Mori, T.; Michinobu, T. High-Performance n-Channel Organic Transistors Using High-Molecular-Weight Electron-Deficient Copolymers and Amine-Tailed Self-Assembled Monolayers. *Adv. Mater.* **2018**, *30*, 1707164. [[CrossRef](#)] [[PubMed](#)]
36. Yan, Z.; Sun, B.; Li, Y. Novel stable (3E,7E)-3,7-bis(2-oxindolin-3-ylidene)-benzo [1,2-*b*:4,5-*b'*]difuran-2,6(3*H*,7*H*)-dione based donor-acceptor polymer semiconductors for n-type organic thin film transistors. *Chem. Commun.* **2013**, *49*, 3790–3792. [[CrossRef](#)]
37. Lei, T.; Dou, J.-H.; Cao, X.-Y.; Wang, J.-Y.; Pei, J. A BDOPV-Based Donor-Acceptor Polymer for High-Performance n-Type and Oxygen-Doped Ambipolar Field-Effect Transistors. *Adv. Mater.* **2013**, *25*, 6589–6593. [[CrossRef](#)]
38. Lei, T.; Dou, J.-H.; Cao, X.-Y.; Wang, J.-Y.; Pei, J. Electron-Deficient Poly(*p*-phenylene vinylene) Provides Electron Mobility over 1 cm<sup>2</sup> V<sup>-1</sup> s<sup>-1</sup> under Ambient Conditions. *J. Am. Chem. Soc.* **2013**, *135*, 12168–12171. [[CrossRef](#)]
39. Lei, T.; Xia, X.; Wang, J.-Y.; Liu, C.-J.; Pei, J. “Conformation Locked” Strong Electron-Deficient Poly(*p*-Phenylene Vinylene) Derivatives for Ambient-Stable n-Type Field-Effect Transistors: Synthesis, Properties, and Effects of Fluorine Substitution Position. *J. Am. Chem. Soc.* **2014**, *136*, 2135–2141. [[CrossRef](#)]
40. Shi, K.; Zhang, F.; Di, C.-A.; Yan, T.-W.; Zou, Y.; Zhou, X.; Zhu, D.; Wang, J.-Y.; Pei, J. Toward High Performance n-Type Thermoelectric Materials by Rational Modification of BDPPV Backbones. *J. Am. Chem. Soc.* **2015**, *137*, 6979–6982. [[CrossRef](#)]

41. Zhou, X.; Ai, N.; Guo, Z.-H.; Zhuang, F.-D.; Jiang, Y.-S.; Wang, J.-Y.; Pei, J. Balanced Ambipolar Organic Thin-Film Transistors Operated under Ambient Conditions: Role of the Donor Moiety in BDOPV-Based Conjugated Copolymers. *Chem. Mater.* **2015**, *27*, 1815–1820.
42. Zheng, Y.-Q.; Lei, T.; Dou, J.-H.; Xia, X.; Wang, J.-Y.; Liu, C.-J.; Pei, J. Strong Electron-Deficient Polymers Lead to High Electron Mobility in Air and Their Morphology-Dependent Transport Behaviors. *Adv. Mater.* **2016**, *28*, 7213–7219. [[PubMed](#)]
43. Zhao, X.; Madan, D.; Cheng, Y.; Zhou, J.; Li, H.; Thon, S.M.; Bragg, A.E.; DeCoster, M.E.; Hopkins, P.E.; Katz, H.E. High Conductivity and Electron-Transfer Validation in an n-Type Fluoride-Anion-Doped Polymer for Thermoelectrics in Air. *Adv. Mater.* **2017**, *29*, 1606928.
44. Zheng, Y.-Q.; Yao, Z.-F.; Lei, T.; Dou, J.-H.; Yang, C.-Y.; Zou, L.; Meng, X.; Ma, W.; Wang, J.-Y.; Pei, J. Unraveling the Solution-State Supramolecular Structures of Donor-Acceptor Polymers and their Influence on Solid-State Morphology and Charge-Transport Properties. *Adv. Mater.* **2017**, *29*, 1701072.
45. Shi, K.; Zhang, W.; Gao, D.; Zhang, S.; Lin, Z.; Zou, Y.; Wang, L.; Yu, G. Well-Balanced Ambipolar Conjugated Polymers Featuring Mild Glass Transition Temperatures Toward High-Performance Flexible Field-Effect Transistors. *Adv. Mater.* **2018**, *30*, 1705286.
46. Wang, F.; Dai, Y.; Wang, W.; Lu, H.; Qiu, L.; Ding, Y.; Zhang, G. Incorporation of Heteroatoms in Conjugated Polymers Backbone toward Air-Stable, High-Performance n-Channel Unencapsulated Polymer Transistors. *Chem. Mater.* **2018**, *30*, 5451–5459.
47. Frisch, M.J.; Trucks, G.W.; Schlegel, H.B.; Scuseria, G.E.; Robb, M.A.; Cheeseman, J.R.; Scalmani, G.; Barone, V.; Petersson, G.A.; Nakatsuji, H.; et al. *Gaussian 16*; Gaussian, Inc.: Wallingford, CT, USA, 2016.



© 2020 by the authors. Licensee MDPI, Basel, Switzerland. This article is an open access article distributed under the terms and conditions of the Creative Commons Attribution (CC BY) license (<http://creativecommons.org/licenses/by/4.0/>).